Control of Stripelike and Hexagonal Self-Assembly of Gold Nanoparticles by the Tuning of Interactions between Triphenylene Ligands

ARTICLE *in* JOURNAL OF THE AMERICAN CHEMICAL SOCIETY · DECEMBER 2007

Impact Factor: 12.11 · DOI: 10.1021/ja073518c · Source: PubMed

J|A|C|S
ARTICLES
Published on Web 10/25/2007

Control of Stripelike and Hexagonal Self-Assembly of Gold Nanoparticles by the Tuning of Interactions between Triphenylene Ligands

Zhongrong Shen,[†] Mami Yamada,[†,‡,§] and Mikio Miyake*[,†]

Contribution from the School of Materials Science, Japan Advanced Institute of Science and Technology, 1-1, Asahidai, Nomi-shi, Ishikawa, 923-1292, Japan, and PRESTO/Japan Science and Technology Agency, 4-1-8 Honcho Kawaguchi, Saitama, 332-0012, Japan

Received May 17, 2007; E-mail: miyake@jaist.ac.jp

Abstract: We describe the self-assembly of gold nanoparticles (Au NPs) protected with newly synthesized discotic liquid crystalline molecules of hexaalkoxy-substituted triphenylene (TP) in mixed toluene/methanol solvent. The stripelike (i.e., 2D consisting of linear 1D in stripe) self-assembly is realized successfully by the aid of $\pi-\pi$ stacking of TP ligand on Au NPs. The smaller Au NPs with TP (AuTP) or the longer alkyl chain between TP and the gold core provide more free spaces among TP moieties. These spaces allow easy insertion of TP on adjacent AuTPs to lead an interparticle $\pi-\pi$ interaction to form the stripelike arrangement. The solvent hydrophilicity can also serve as a controlled index to tune arrangement among stripelike, hexagonal close packed (*hcp*), or disorder. We have changed the solvent hydrophilicity by changing the ratio of methanol to toluene, which affects the balance of solution of AuTP (in toluene) and deposition (in methanol). The larger space between TPs and appropriate solvent hydrophilicity realize stripelike self-assembly caused by a strong $\pi-\pi$ interaction between TPs, which was characterized by TEM, as well as fluorescence, dynamic light scattering, and ^{1}H NMR spectra.

1. Introduction

Fabrication of nanoparticles (NPs) in a desired form has received significant attention in recent years.[1] Especially, the development of highly anisotropic assembly is desired. For instance, 1D arrays of NPs have potential for the directional transfer of photons and/or electrons, due to a dramatic increase of particle−particle interaction, leading to construction of nanoscale devices,[2] such as plasmon waveguides, magnetic logic, quantum cellular automata, and Coulomb blockade devices.[3−6] Existing methods to fabricate 1D arrangement can be classified as dip-pen nanolithography (DPN),[7] electron beam lithography (EBL),[8−11] templates and self-assembly of NPs. The proposed lithography techniques have found limited usage due to their low speed and high cost. Templates to direct NPs into 1D arrangements have been reported extensively by using linear molecules, such as CNT, DNA, RNA, and polymer,[12−15] as well as nanoporous alumina,[16] or stripelike grooves.[17] Our group has previously reported the effectiveness of a ridge-and-valley structure constructed by a NaCl crystal to array gold NPs into a 1D structure.[18] With these template methods, it is difficult to tune an ordering pattern in a desired 1D and 2D hexagonal close packed (*hcp*) structure. Self-assembly is emerging as an elegant, "bottom-up" method for fabricating nanostructured materials. There are only limited reports of the 1D arrangement of nonmagnetic NPs; for example, a stripe structure of linear 1D by dendron thiol ligand,[19] 1D arrangements of NPs induced by rodlike liquid crystalline (LC) thiol ligand,[20] dipolar moments,[21−23] hydrophobic effect,[24] π-conjugated OPV tapes,[25] placing target

[†] Japan Advanced Institute of Science and Technology.
[‡] Japan Science and Technology Agency.
[§] Present address: Tokyo University of Agriculture and Technology.

(1) Schmid, G. *Nanoparticle: From Theory to Application*; Wiley-VCH: Weinheim, 2004.
(2) Berry, V.; Saraf, R. F. *Angew. Chem., Int. Ed.* **2005**, *44*, 6668−6673.
(3) Maier, S. A.; Kik, P. G.; Atwater, H. A.; Meltzer, S.; Harel, E.; Koel, B. E.; Requicha, A. A. G. *Nat. Mater.* **2003**, *2*, 229−232.
(4) Cowburn, R. P.; Welland, M. E. *Science* **2000**, *287*, 1466−1468.
(5) Imre, A.; Csaba, G.; Ji, L.; Orlov, A.; Bernstein, G. H.; Porod, W. W. *Science* **2006**, *311*, 205−208.
(6) Chen, W.; Ahmed, H.; Nakazoto, K. *Appl. Phys. Lett.* **1995**, *66*, 3383−3384.
(7) Piner, R. D.; Zhu, J.; Xu, F.; Hong, S.; Mirkin, C. A. *Science* **1999**, *283*, 661−663.
(8) Fischer, U. C.; Zingsheim, H. P. J. *Vac. Sci. Technol.* **1981**, *19*, 881−885.
(9) Deckman, H. W.; Dunsmuir, J. H. J. *Vac. Sci. Technol. B* **1983**, *1*, 1109−1112.
(10) Lercel, M. J.; Craighead, H. G.; Parikh, A. N.; Seshadri, K.; Allara, D. L. *Appl. Phys. Lett.* **1996**, *68*, 1504−1506.
(11) Lee, K-B.; Park, S-J.; Mirkin, C. A.; Smith, J. C.; Mrksich, M. *Science* **2002**, *295*, 1702−1705.
(12) Niemeyer, C. M. *Curr. Opin. Chem. Biol.* **2000**, *4*, 609−618.
(13) Wyrwa, D.; Beyer, N.; Schmid, G. *Nano Lett.* **2002**, *2*, 419−421.
(14) Liu, Y.; Meyer-Zaika, W.; Frauzka, S.; Schmid, G.; Tsoli, M.; Kuhn, H. *Angew. Chem., Int. Ed.* **2003**, *42*, 2853−2857.
(15) Koyfman, A. Y.; Braun, G.; Magonov, S.; Chworos, A.; Reich, N. O.; Jaeger, L. *J. Am. Chem. Soc.* **2005**, *127*, 11886−11887.
(16) Schmid, G. *J. Mater. Chem.* **2002**, *12*, 1231−1238.
(17) Cheng, J. Y.; Zhang, F.; Chuang, V. P.; Mayes, A. M.; Ross, C. A. *Nano Lett.* **2006**, *6*, 2099−2103.
(18) Teranishi, T.; Sugawara, A.; Shimizu, T.; Miyake, M. *J. Am. Chem. Soc.* **2002**, 4210−4211.
(19) Nakao, S.; Torigoe, K.; Kon-No, K.; Yonezawa, T. *J. Phys. Chem. B* **2002**, *106*, 12097−12100.
(20) In, I.; Jun, Y. W.; Kim, Y. J.; Kim, S. Y. *Chem. Commun.* **2005**, 800−801.
(21) Ma, H.; Li, G.; Zhang, J.; Shen, Q.; Wang, X. *ChemPhysChem* **2004**, *5*, 713−716.
(22) Huang, S.; Ma, H.; Zhang, X.; Yong, F.; Feng, X.; Pan, W.; Wang, X.; Wang, Y.; Chen, S. *J. Phys. Chem. B* **2005**, *109*, 19823−19830.
(23) Tang. Z.; Kotov, N. A.; Giersig, M. *Science* **2002**, *297*, 237−240.

molecules specifically at two diametrically opposed positions of NP,[26] and controlling the surfactant population.[27] However, these previously reported methods give limited quasi one-dimensional structure.

We have been focusing our attention on the function of an organic ligand used as a protective agent of metal NPs. We succeeded in arranging small Au NPs (less than 2 nm diameter) in 2D by the aid of $\pi-\pi$ interaction of bisimidazole pyridine ligand in 2000.[28] Many groups are interested in the $\pi-\pi$ interaction of organic protective agents to control various types of assembly of NPs,[29] for example, spherical aggregates by terthiophene[30] and 2D assembly by pyrene units[31,32] or by thiophene ligands.[33] 1D assemblies of NPs can also be realized by fixation on the 1D matrix by $\pi-\pi$ interactions.[34] To the best of our knowledge, no report has appeared yet for the 1D stripelike arrangement of NPs induced by interactions of organic protective agents.

In the present study, we adopt the newly synthesized discotic liquid crystal molecule, triphenylene (TP),[35] as a protective agent of Au NPs to induce tunable self-assembly via $\pi-\pi$ interaction, because disc-shaped (discotic) liquid crystals (DLCs)[36] are very effective in forming supramolecular assemblies of columnar phases.[37−39] We attach importance to the primary findings that the circumstances of an NP system play a key role for the assembled NPs.[40] When organic ligands are not well dissolved, NPs tend to coagulate and deposit in solution. Amphiphilic molecules are gathered into micelles, layers, or even linear wires[26,41,42] as a result of competing molecular interactions in different solvents. Recently, we reported a convenient method to control the shape of Pt nanocrystals by changing solvent polarity in different ratios of water−toluene−*N*,*N*-dimethylformamide (DMF).[43] Single crystalline platinum nanowires of 2 nm in diameter have been obtained in a low polarity solution, while only platinum NPs have been obtained in a high polarity solution. That is, solvent could be a very simple, advantageous parameter in tuning the assembly, even for organic ligand-stabilized NPs. We synthesized several Au NPs, which were stabilized by different TPD*n* molecules (Figure 1a) to change the free space around Au NPs. The large free space around TP ligands can be realized by reducing the core size (Figure 1b) or using a long alkyl chain (Figure 1c). To deeply understand the crucial factors for the specific arrangement of Au NPs by the tuning of the $\pi-\pi$ interaction of DLCs will give a clue to constructing new composite functional materials consisting of metal NPs.

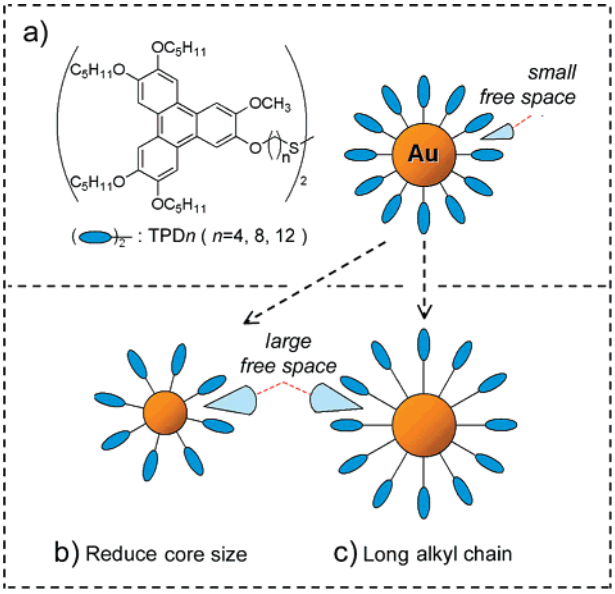

Figure 1. Three strategies to construct 1D arrangement of NPs: (a) Synthesize molecules with triphenylene ligands (TPD*n*, $n = 4$, 8 or 12) and gold nanoparticles stabilized by TPD*n*; enlarge free space between triphenylene moieties: (b) reduce the core size; (c) or use long alkyl chain.

2. Experimental Section

2.1. Chemicals. All chemicals were purchased from Sigma-Aldrich, Wako Chemical, and Kanto Chemical. All were analytical-grade reagents and used as received unless otherwise noted. 2-Hydroxy-3-methoxy-6,7,10,11-tetrakis-pentoxy-triphenylene (**1**, Scheme 1) was prepared according to the literature.[44]

2.1.1. Synthesis of 2-(*n*-Bromo-*n*-alkoxy)-3-methoxy-6,7,10,11-tetrakis-pentyloxy-triphenylene (2, $n = 4$, 8, 12). Compound **1** (1.0 g, 1.0 equiv), potassium carbonate (2.7 equiv), α,ω-dibromoalkane (12 equiv), and 30 mL acetone were mixed together and then heated to reflux for 24 h. The mixture was cooled down to room temperature (rt) and then filtered. The solvent was removed under vacuum to produce a white solid. This solid was recrystallized in 60 mL of ethanol twice. The desired compound **2** was obtained as a white solid (81−90% yield).

2.1.1.1. Characterization of 2-(4-Bromo-butoxy)-3-methoxy-6,7,-10,11-tetrakis-pentyloxy-triphenylene (2a, $n = 4$). ^{1}H NMR (300M, $CDCl_3$): δ 7.84−7.81 (m, 6H), 4.23 (t, 10H), 4.10 (s, 3H), 3.59 (t, 2H), 2.21−2.14 (m, 4H), 2.01−1.92 (m, 8H), 1.63−1.41 (m, 16H),

(24) Zubarev. E. R.; Xu, J.; Sayyad, A.; Gibson, J. D. *J. Am. Chem. Soc*. **2006**, *128*, 15098−15099.
(25) van Herrikhuyzen, J.; George, S. J.; Vos, M. R. J.; Sommerdijk, N. A. J. M.; Ajayaghosh, A.; Meskers, S. C. J.; Schenning, A. P. H. J. *Angew. Chem., Int. Ed.* **2007**, *46*, 1825−1828.
(26) DeVries, G. A.; Brunnbauer, M.; Hu, Y.; Jackson, A. M.; Long, B.; Neltner, B. T.; Uzun, O.; Wunsch, B. H.; Stellacci, F. *Science* **2007**, *315*, 358−361.
(27) Zhang, Y.-X.; Zeng, H.-C. *J. Phys. Chem. B*, **2006**, *110*, 16812−16815.
(28) Teranishi, T.; Haga, M.; Shiozawa, Y.; Miyake, M. *J. Am. Chem. Soc.* **2000**, *122*, 4237−4238.
(29) (a) Yang, Z.; Gu, H.; Zhang, Y.; Wang, L.; Xu, B. *Chem. Commun.* **2004**, 208−209. (b) Toledano, S.; Williams, R. J.; Jayawarna, V.; Ulijn, R. V. *J. Am. Chem. Soc.* **2006**, *128*, 1070−1071. (c) Mahler, A.; Reches, M.; Rechter, M.; Cohen, S.; Gazit, E. *Adv. Mater.* **2006**, *18*, 1365−1370. (d) Schnepp, Z. A. C.; Gonzalez-McQuire, R.; Mann, S. *Adv. Mater.* **2006**, *18*, 1869−1872. (e) Laromaine, A.; Koh, L.; Murugesan, M.; Ulijn, R. V.; Stevens, M. M. *J. Am. Chem. Soc.* **2007**, *129*, 4156−4157.
(30) Jin, J.; Iyoda, T.; Cao, C.; Song, Y.; Jiang, L.; Li, T.; Zhu, D. *Angew. Chem., Int. Ed.* **2001**, *40*, 2135−2138.
(31) Wang, T.; Zhang, D.; Xu, W.; Yang, J.; Han, R.; Zhu, D. *Langmuir* **2002**, *18*, 1840−1848.
(32) Ipe, B. I.; Thomas, K. G. *J. Phys. Chem. B* **2004**, *108*, 13265−13272.
(33) Nirmal, R. G.; Kavitha, A. L.; Berchmans, S.; Yegnaraman, V. *J. Nanosci. Nanotechnol.* **2007**, *7*, 2116−2124.
(34) (a) Wang, F.; Han, M.-Y.; Mya, K. Y.; Wang, Y.; Lai, Y.-H. *J. Am. Chem. Soc.* **2005**, *127*, 10350−10355. (b) Jung, J. H.; Kim, T. W.; Song, M. S.; Kim, Y.-H.; Yoo, K. H. *J. Appl. Phy.* **2007**, *101*, 093708/1−4. (c) Ozawa, H.; Kawao, M.; Tanaka, H.; Ogawa, T. *Langmuir* **2007**, *23*, 6365−6371.
(35) Markovitsi, D.; Germain, A.; Millié, P.; Lécuyer, P.; Gallos, L. K.; Argyrakis, P.; Bengs, H.; Ringsdorf, H. *J. Phys. Chem.* **1995**, *99*, 1005−1017.
(36) Chandrasekhar, S.; Sadashiva, B. K.; Suresh, K. A. *Pramana* **1977**, *9*, 471−480.
(37) Adam, D.; Schuhmacher, P.; Simmerer, J.; Haussling, L.; Siemensmeyer, K.; Etzbach, K. H.; Ringsdorf, H.; Haarer, D. *Nature* **1994**, *371*, 141−143.
(38) Zhang, X.; Xie, P.; Shen, Z.; Jiang, J.; Zhu, C.; Li, H.; Zhang, T.; Han, C. C.; Wan, L.; Yan, S.; Zhang, R. *Angew. Chem., Int. Ed.* **2006**, *45*, 3112−3116.
(39) Cui, L.; Miao, J.; Zhu, L. *Macromolecules* **2006**, *39*, 2536−2545.
(40) Yamada, M.; Shen, Z.; Miyake, M. *Chem. Commun*. **2006**, 2569−2571
(41) Antonietti, M.; Göltner, C. *Angew. Chem., Int. Ed.* **1997**, *36*, 910−928.
(42) Jin, W.; Fukushima, T.; Kosaka, A.; Niki, M.; Ishii, N.; Aida, T. *J. Am. Chem. Soc*. **2005**, *127*, 8284−8285.
(43) Shen, Z.; Yamada, M.; Miyake, M. *Chem. Commun*. **2007**, 245−247
(44) Ba, C.; Shen, Z.; Gu, H.; Guo, G.; Xie, P.; Zhang, R. *Liq. Cryst.* **2003**, *30*, 391−397.

Scheme 1. Synthetic Procedures for Preparation of TPD*n* Ligands

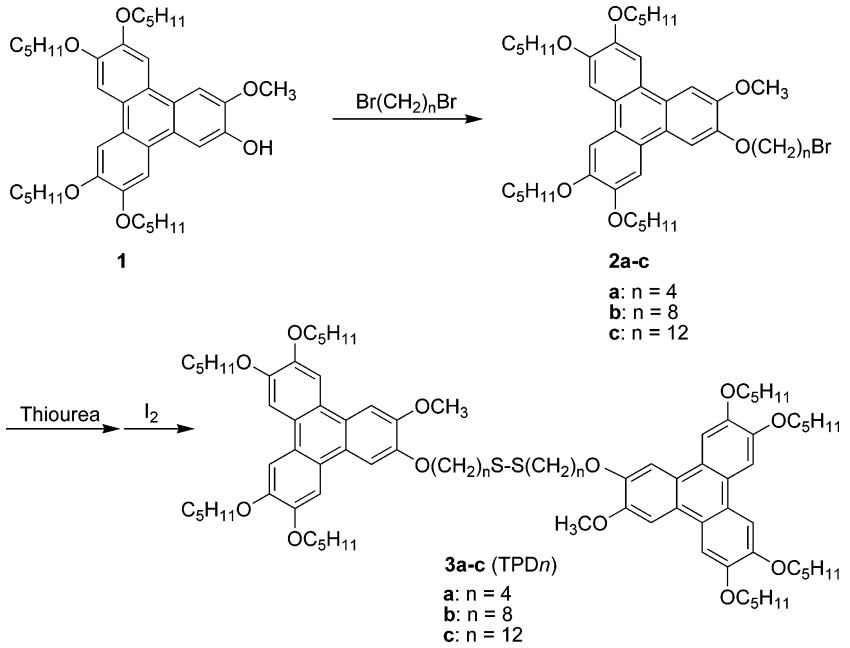

Table 1. Mean Diameters and Standard Deviations of a Series of AuTP NPs Synthesized at Various TPD*n*/Au Molar Ratios

compound	ligand	TPD*n*/Au (mol/mol)	mean diameter (nm)	SD (nm)
AuTP4-2.9	TPD4	0.5	2.9	0.7
AuTP8-2.4	TPD8	0.5	2.4	0.3
AuTP8-2.8	TPD8	0.2	2.8	0.4
AuTP8-3.0	TPD8	0.1	3.0	0.3
AuTP12-2.8	TPD12	0.5	2.8	0.3

0.98 (t, 12H). FT-IR (KBr) 2954 (Ar—H), 2929, 2858, 1618 (C═C), 1517, 1436, 1388, 1261, 1054 (C—O), 837 cm^{-1}. Anal. Calcd for $C_{43}H_{61}BrO_6$: C, 68.51; H, 8.16. Found: C, 68.41; H, 7.89.

2.1.1.2. Characterization of 2-(8-Bromo-octoxy)-3-methoxy-6,7,-10,11-tetrakis-pentyloxy-triphenylene (2b, *n* = 8). ^{1}H NMR (300M, $CDCl_3$): δ 7.86−7.80 (m, 6H), 4.24 (t, 10H), 4.10 (s, 3H), 3.42 (t, 2H), 2.00−1.81 (m, 12H), 1.61−1.40 (m, 24H), 0.98 (t, 12H). FT-IR (KBr) 2954 (Ar—H), 2929, 2858, 1618 (C═C), 1517, 1436, 1388, 1261, 1054 (C—O), 837 cm^{-1}. Anal. Calcd for $C_{47}H_{69}BrO_6$: C, 69.70; H, 8.59. Found: C, 70.29; H, 9.01.

2.1.1.3. Characterization of (2-(12-Bromo-dodecanoxy)-3-methoxy-6,7,10,11-tetrakis-pentyloxy-triphenylene) (2c, *n* = 12). ^{1}H NMR (300M, $CDCl_3$): δ 7.84−7.81 (m, 6H), 4.23 (t, 10H), 4.10 (s, 3H), 3.40 (t, 2H), 1.98−1.92 (m, 10H), 1.91−180 (m, 2H), 1.60−1.26 (m, 32H), 0.98 (t, 12H). FT-IR (KBr) 2954 (Ar—H), 2929, 2858, 1618 (C═C), 1517, 1436, 1388, 1261, 1054 (C—O), 837 cm^{-1}. Anal. Calcd for $C_{51}H_{77}BrO_6$: C, 70.73; H, 8.96. Found: C, 71.02; H, 8.63.

2.1.2. Synthesis of 4-(3-Methoxy-6,7,10,11-tetrakis-pentyloxy-triphenylen-2-yloxy)-alkyl Disulfide (3, TPD*n*). Compound **2** (1.0 g, 1.0 equiv), thiourea (0.37 g, 3.6 equiv), and 50 mL of ethanol were mixed under nitrogen and then heated to reflux and kept for 6−12 h until the reaction finished, as detected by TLC. Then the mixture was cooled to rt, and a sodium hydroxide solution (10%, 3.6 equiv) was added. After refluxing for approximately 4 h, the system was cooled to rt, and the pH was adjusted to 7 with diluted sulfuric acid. The system was cooled to 0 °C for 2 h, filtered, washed with water, and recrystallized in 50 mL of ethanol. The intermediate product was obtained as a yellow solid without further purification. For the total intermediate product, 15 mL of methanol, 50 mL of ethanol, aq. potassium hydroxide (10% 1.2 equiv), and iodine (0.6 equiv) were mixed in a 100 mL flask and then heated to reflux overnight. After cooling to rt, the solvent was removed under vacuum, and then the residue was dissolved into 50 mL of ethyl acetate and washed with 25 mL of water twice. The solvent was removed, and the compound was recrystallized by 50 mL of ethanol. The final product **3** (**TPD*n***) was obtained as a pale yellow solid. (75−80% yield).

2.1.2.1. Characterization of 4-(3-Methoxy-6,7,10,11-tetrakis-pentyloxy-triphenylen-2-yloxy)-alkyl Disulfide (3a, *n* = 4, TPD4). ^{1}H NMR (300M, $CDCl_3$): δ 7.80−7.75 (m, 12H), 4.23 (t, 20H), 4.07 (s, 6H), 2.87 (t, 4H), 2.056 (m, 8H), 1.98−1.92 (m, 16H), 1.60−1.40 (m, 32H), 0.99 (t, 24H). FTIR (KBr) 2954 (Ar—H), 2927, 2858, 1618 (C═C), 1517, 1508, 1434, 1263, 1167, 1051 (C—O), 835 cm^{-1}. Anal. Calcd for $C_{86}H_{122}O_{12}S_2$: C, 73.15; S, 4.54; H, 8.71. Found: C, 73.35; S, 4.19; H, 8.87

2.1.2.2. Characterization of 8-(3-Methoxy-6,7,10,11-tetrakis-pentyloxy-triphenylen-2-yloxy)-octanyl Disulfide (3b, *n* = 8, TPD8). ^{1}H NMR (300M, $CDCl_3$): δ 7.84−7.80 (m, 12H), 4.23 (t, 20H), 4.09 (s, 6H), 2.69 (t, 4H), 1.98−1.92 (m, 20H), 1,71−1.68 (m, 4H), 1.60−1.53 (m, 22H), 1.49−1.38 (m, 28H), 0.99 (t, 24H). FTIR (KBr) 2954 (Ar—H), 2927, 2858, 1618 (C═C), 1517, 1508, 1434, 1263, 1167, 1051 (C—O), 835 cm^{-1}. Anal. Calcd for $C_{94}H_{138}O_{12}S_2$: C, 74.10; S, 4.21; H, 9.13. Found: C, 74.33; S, 3.96; H, 8.85

2.1.2.3. Characterization of 12-(3-Methoxy-6,7,10,11-tetrakis-pentyloxy-triphenylen-2-yloxy)-dodecyl Disulfide (3c, *n* = 12, TPD12). ^{1}H NMR (300M, $CDCl_3$): δ 7.84−7.80 (m, 12H), 4.23 (t, 20H), 4.09 (s, 6H), 2.67 (t, 4H), 1.97−1.90 (m, 20H), 1,70−1.62 (m, 4H), 1.60−1.22 (m, 64H), 0.97 (t, 24H). FTIR (KBr) 2954 (Ar—H), 2927, 2858, 1618 (C═C), 1517, 1508, 1434, 1263, 1167, 1051 (C—O), 835 cm^{-1}. Anal. Calcd for $C_{102}H_{154}O_{12}S_2$: C, 74.86; S, 3.92; H, 9.49. Found: C, 75.30; S, 3.79; H, 9.54.

2.1.3. Synthesis of TPD*n* Protected Gold NPs. The TPD*n* protected gold NPs (AuTPs) were synthesized in a homogeneous phase of DMF/water by the $NaBH_4$ reduction of $HAuCl_4$ in the presence of a series of TPD*n* ligands, on the basis of our previous study.[40] For a typical reaction, 1 mL of 10 mM aq. $HAuCl_4$ and 40 mL of DMF were added to 8.2 mg of TPD12 (TPD12/Au = 0.5 in molar ratio) in DMF. After heating to 60 °C, 1 mL of 0.1 M aq. $NaBH_4$ was introduced to the mixture with 2 h of vigorous stirring. 40 mL of water were added, and then, the solution was extracted with 20 mL of toluene. The separated toluene phase was washed with 10 mL of water, and the solid was precipitated by the addition of methanol. This precipitation process was

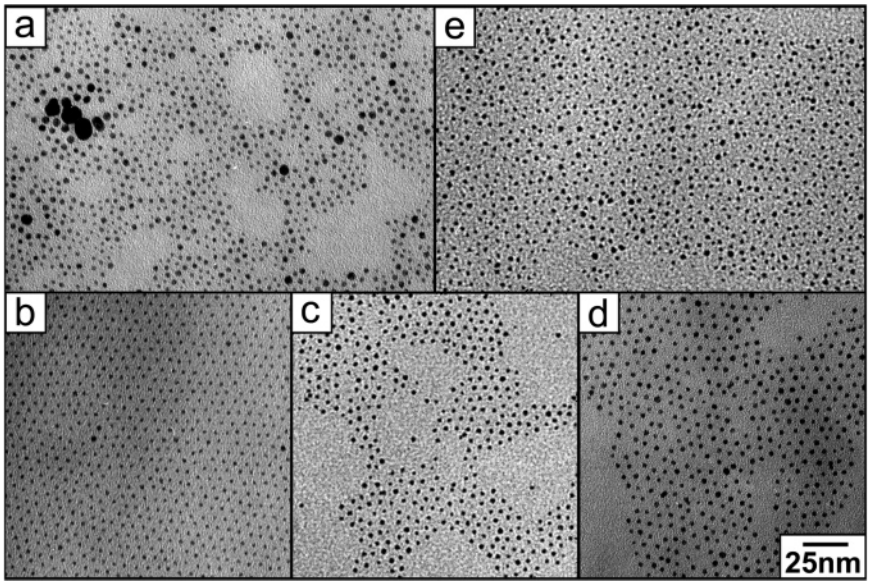

Figure 2. TEM images of (a) AuTP4-2.9, (b) AuTP8-2.4, (c) AuTP8-2.8, (d) AuTP8-3.0, and (e) AuTP12-2.8. Scroll bar is 25 nm, and the magnification is the same for a−e.

repeated 3 times, followed by washing with excess methanol to give a black powder of Au NPs protected by TP12. Other gold NPs with different core sizes or different ligands can be synthesized with the appropriate molar ratio of TPD*n*/Au (as shown in Table 1) and with the same amount of aq. $HAuCl_4$ and DMF in the same procedure. The product is abbreviated as shown here; AuTP12−2.8 means the gold NPs are protected by TP12 and the average size of the gold core is 2.8 nm.

2.1.4. Preparation of the TEM Grid. For the characterization of Au NPs by TEM, a carbon-supported copper grid (Okenshoji, Model: STEM100 Cu grid) was used. The grid was stored in a desiccator and used without any treatment. A methanol−toluene solution containing AuTP (1.0×10^{-5}g/mL) was aged for more than 2 days and dropped (~0.05 mL) onto the grid. All grids were dried naturally for 1 day before the TEM observation.

2.2. Characterization. ^{1}H NMR spectra were recorded with $CDCl_3$ solutions on a Varian 300 (300 MHz) spectrometer. Samples were analyzed for carbon, hydrogen, and sulfur on a Vario EL II elemental analyzer. FT-IR spectra were recorded on an ISF-66V spectrometer as thin films on KBr plates. TEM images were obtained by using transmission electron microscopy (H7100, Hitachi, 100 kV). UV−vis and fluorescence spectra were measured in a concentration of 1.0×10^{-5} g/mL, using a MultiSpec-1500 Shimadzu spectrophotometer and an RF-5300PC Shimadzu spectrofluorophotometer, respectively. Dynamic light scattering was measured with a ZetaSizer Nano (Sysmex) for a solution containing AuTP12-2.8 (1.0×10^{-5}g/mL) at different aging times (fresh and 2 days later).

3. Results and Discussion

3.1. Characterization of AuTPs and Their Arrangement by TEM. Table 1 presents the mean diameters and standard deviations of Au NPs prepared at various TPD*n*/Au molar ratios estimated based on TEM observation (Figure 2). The diameter of Au NPs decreased from 3.0 to 2.4 nm with an increase in the amount of the protective agent, TPD8 (0.1−0.5 molar ratio of TPD8/Au), where the standard deviations in the mean diameter varied slightly (0.3−0.4 nm). When different kinds of TPD*n* (n = 4, 8, 12) were used, the diameter and standard deviation changed significantly. By using TPD4 as a protective ligand, only polydispersed Au NPs (standard deviation of 0.7 nm) were produced, even under a high molar ratio of TPD4/Au (0.5). Furthermore, aggregations of AuTP4-2.9 are observed in TEM images (Figure 2a). The less stable behavior of AuTP4-2.9 may be induced by the low coverage of TPD4, originating from the bulkiness of triphenylene moiety and the short linkage (C_4) between triphenylene moiety and gold core (see Figure 1c). Ligands with a longer alkyl chain tend to produce larger Au NPs at the same ligand/Au molar ratio, contrary to the previously reported results:[45] AuTP12-2.8 and AuTP8-2.4 have 2.8 and 2.4 nm diameters, respectively (see Table 1), which were confirmed by duplicate experiments. A possible reason is the curled linkage and interaction among TP moieties. Figure 3 shows the representative UV−vis spectra of AuTPs in chloroform. The absorbance at 283−285 nm is assigned to the degenerate S0 → S4 transition of TP moieties.[35,46] Surface plasmon resonance bands around 520 nm were clearly observed for AuTP4-2.9 (Figure 3a), indicating the presence of larger-sized NPs, in accordance with the TEM image in Figure 2a. For AuTP8-2.4, -2.8, -3.0 and AuTP12-2.8 (Figure 3b−e), the

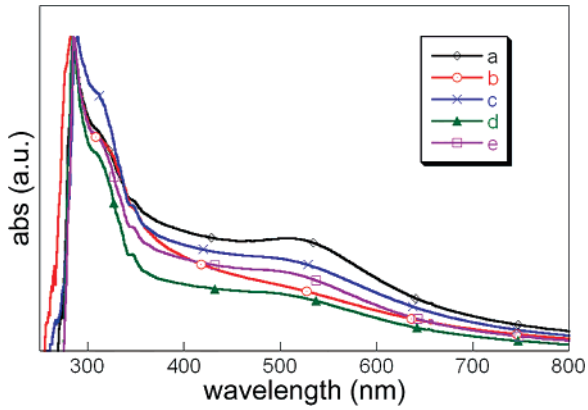

Figure 3. UV−vis spectra of (a) AuTP4-2.9, (b) AuTP8-2.4, (c) AuTP8-2.8, (d) AuTP8-3.0, and (e) AuTP12-2.8 in chloroform with a concentration of 1.0×10^{-5} g/mL.

(45) Daniel, M.-C.; Astruc, D. *Chem. Rev.* **2004**, *104*, 293−346.
(46) Marguet, S.; Markovitsi, D.; Millié, P.; Sigal, H.; Kumar, S. *J. Phys. Chem. B* **1998**, *102*, 4697−4710.

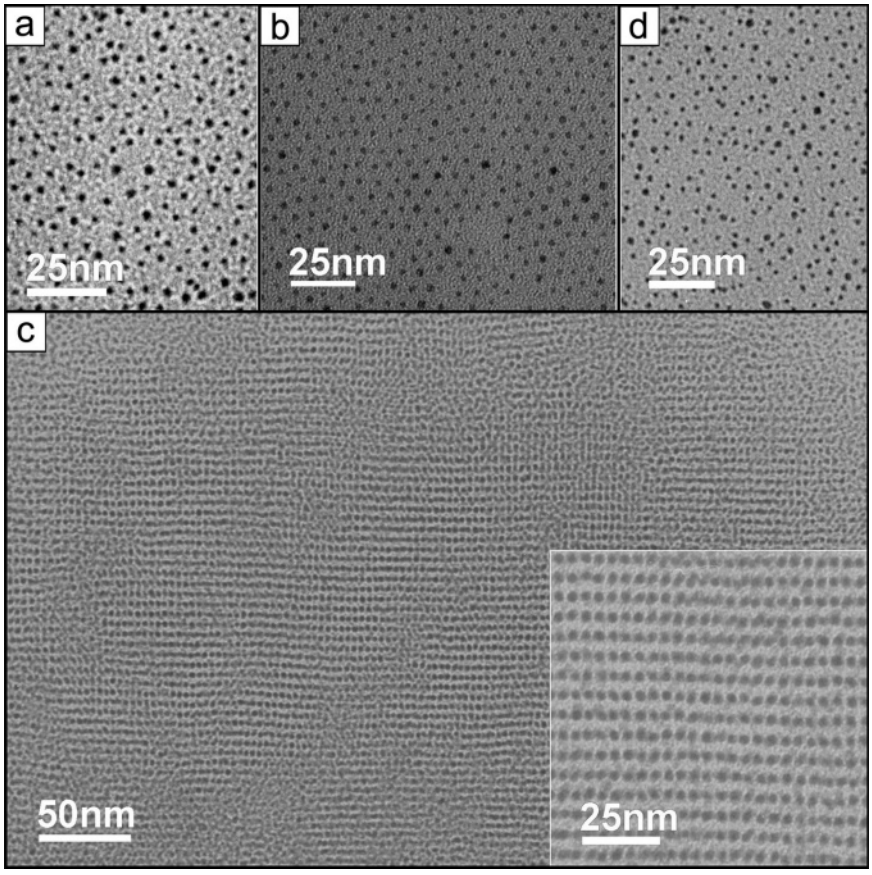

Figure 4. TEM images of AuTP12-2.8 prepared from aged solution stood for 10 days R_{MT} = (a) 1/1 (disorder), (b) 2/1 (*hcp*; interparticle separation is 4.0 nm), (c) 3/1 (stripelike; row spacing is 3.4 nm and interparticle separation in line is 0.9 nm; inset is the enlarged image), and (d) 4/1 (collapse structure).

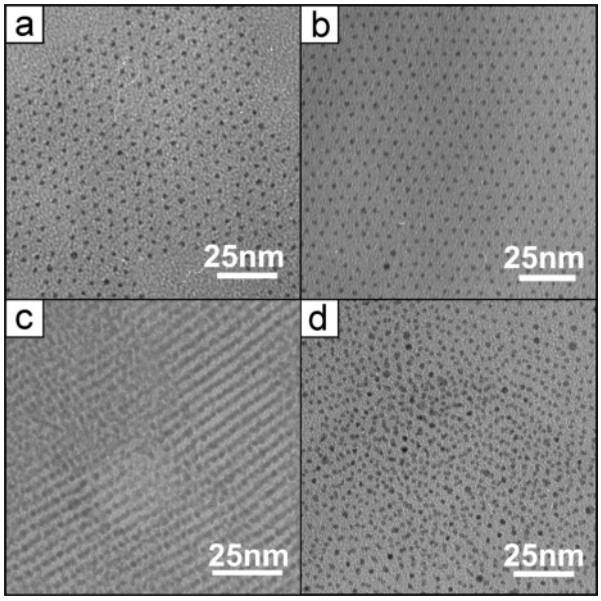

Figure 5. TEM images of AuTP8-2.4 prepared from aged solution stood for 2 days R_{MT} = (a) 0/1 (*hcp*; interparticle separation is 4.2 nm), (b) 1/1 (*hcp*; interparticle separation is 3.2 nm), (c) 2/1 (stripelike; row spacing is 2.6 nm and interparticle separation in line is 0.7 nm), (d) 3/1 (collapse structure).

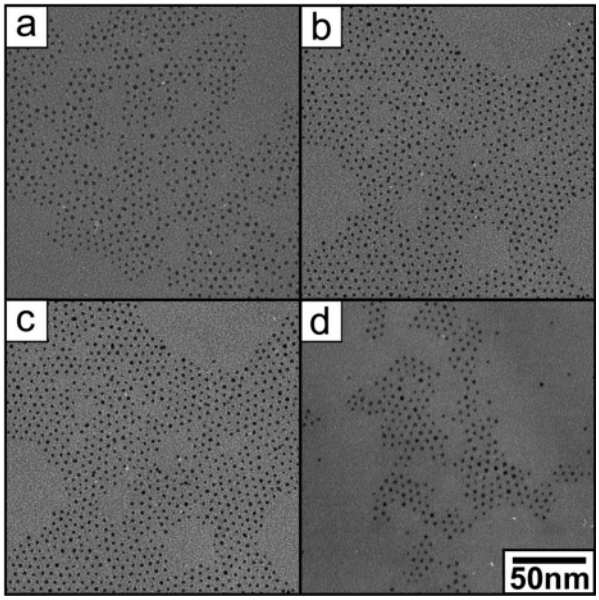

Figure 6. TEM images of AuTP8-2.8 prepared from aged solution stood for 10 days R_{MT} = (a) 1/1, (b) 2/1, (c) 3/1, and (d) 4/1.

surface plasmon resonance band near 520 nm is not obvious, indicating the absence of large particles.[47] These results are consistent with the observation by TEM shown in Figure 2.

(47) Bohren, C. F.; Huffman, D. R. *Absorption and Scattering of Light by Small Particles*; Wiley: New York, 1983.

3.2. Self-Assembled 1D and 2D Arrangements of AuTPs by Solvent Hydrophilicity. Figures 4−6 show TEM images of AuTPs prepared from an aged solution with different R_{MT} values. The R_{MT} value, the ratio of methanol to toluene (v/v), is adopted as a measure of the hydrophilicity index. Figure 4 shows TEM images of the AuTP12-2.8. At R_{MT} = 1/1, AuTP12-2.8 was disordered (Figure 4a), while the *hcp* assembly appears

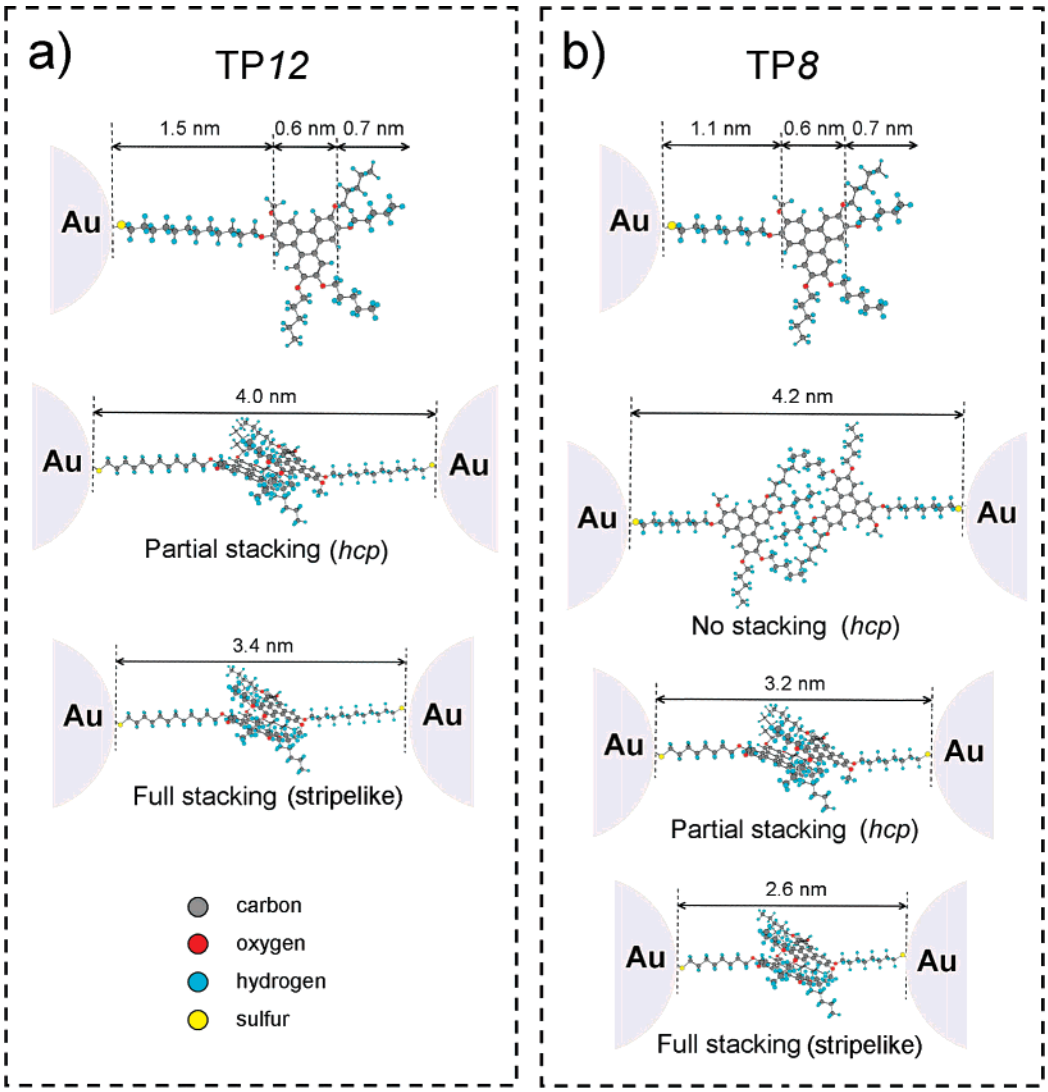

Figure 7. Schematic illustration of (a) TP12 moieties on gold core with partial stacking (d_{int} = 4.0 nm) and full stacking (d_{int} = 3.4 nm); (b) TP8 moieties on gold core without stacking (d_{int} = 4.2 nm), with partial stacking (d_{int} = 3.2 nm), and with full stacking (d_{int} = 2.6 nm). d_{int} is defined as interparticle separation.

for R_{MT} = 2/1 (Figure 4b). When the hydrophilicity of the solvent was further increased (R_{MT} = 3/1), the organization was converted to a stripelike arrangement (2D consisting of linear 1D arranged in parallel stripe, Figure 4c), which spread to a *ca.* 0.5 μm area. On the other hand, the particles were disordered for R_{MT} above 4/1 (Figure 4d). Figure 5 shows TEM images of the AuTP8-2.4 with short methylene chain (from 12 to 8) and small Au core size (from 2.8 to 2.4 nm). When the solvent hydrophilicity was relatively low (R_{MT} = 0/1, 1/1), a clear *hcp* structure was formed (Figure 5a and 5b). When the hydrophilicity of the solvent was further increased (R_{MT} = 2/1), the assembly structure was changed from *hcp* to a stripelike arrangement (Figure 5c). The well-defined superstructure of AuTP8-2.4 disappears with an increase of R_{MT} above 3/1 (Figure 5d), in a manner similar to that observed for AuTP12-2.8 (Figure 4d). Figure 6 shows the TEM image of AuTP8-2.8 with different R_{MT} values (1/1−4/1), where only the *hcp* arrangement appeared at any R_{MT} from 1/1 to 4/1, even after aging for 10 days. It should be mentioned that AuTP8-2.8 has the same methylene-chain length and the larger Au core size compared with those of AuTP8-2.4 (Figure 5) and also has the shorter methylene-chain length and the same Au core size compared with those of AuTP12−2.8 (Figure 4).

Based on the distance between Au NPs observed by TEM (Figures 4−6), we estimate the degree of association of TP12 (Figure 7a) and TP8 (Figure 7b) on adjacent Au NPs by MOPAC. The full molecular length of the TP12 ligand is ca. 2.8 nm, where the C_{12} alkyl chain is 1.5 nm, the aromatic frame of the TP moiety is 0.6 nm, and the surrounding pentoxy group of the TP moiety is 0.7 nm. An interparticle distance of 4.0 nm for *hcp* estimated by the TEM image shown in Figure 4b implies the partial $\pi-\pi$ stacking of TP moieties (Figure 7a). In the case of a stripelike arrangement with a spacing between lines of 3.4 nm (based on Figure 4c), a full $\pi-\pi$ stacking may be realized. A similar MOPAC calculation for TP8 is shown in Figure 7b. The *hcp* arrangement in Figure 5b corresponds to the partial $\pi-\pi$ stacking of TP moieties with an interparticle separation of 3.2 nm. Stripelike arrangement (Figure 5c) with row spacing (2.6 nm) corresponds to the *full* stacking of the TP8 moieties. On the other hand, no $\pi-\pi$ stacking of the TP moiety occurs for 4.2 nm spacing, compatible with the results for AuTP8-2.4 (Figure 5a) and AuTP8-2.8 (Figure 6).

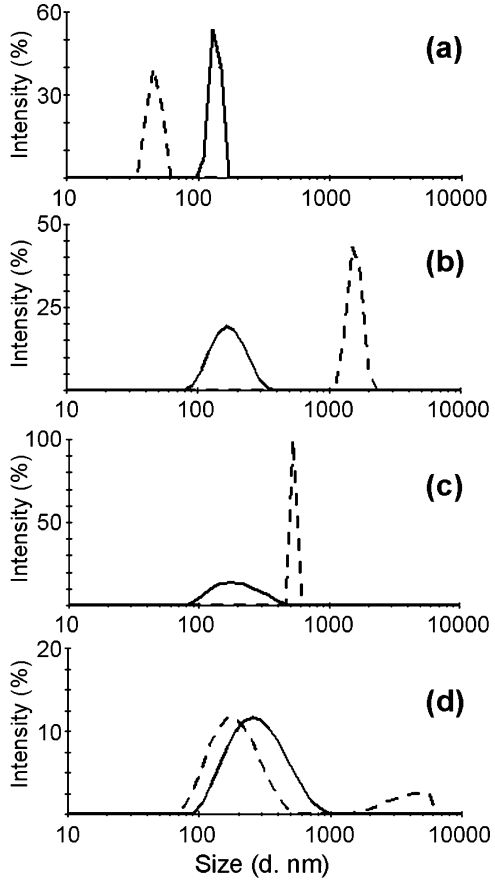

Figure 8. DLS measurement to estimate size of aggregated AuTP12-2.8 at different ratios of methanol to toluene for fresh solution (solid line) and aged solution (2 days, dashed line): (a) $R_{MT} = 1/1$; (b) $R_{MT} = 2/1$; (c) $R_{MT} = 3/1$, and (d) $R_{MT} = 4/1$.

In order to estimate the morphology of aggregation of AuTPs (self-assembly), we measured the dynamic light scattering (DLS) by ZetaSizerNano[48] for the solution of AuTP12-2.8 with different R_{MT} values (Figure 8). The diameter of the aggregate of AuTP12-2.8 was about 100−200 nm for the all fresh solutions with $R_{MT} = 1/1$ to 4/1. After aging for 2 days, the size of aggregation did not increase for the solutions with $R_{MT} = 1/1$ and 4/1 (Figure 8a and 8d, respectively) while it obviously increased for solutions with $R_{MT} = 2/1$ and 3/1 (Figure 8b and 8c, respectively). The diameter of the aggregates are 1480 nm and 531 nm in $R_{MT} = 2/1$ and 3/1, respectively. The solvent systems, which result in the arrangement of AuTPs as *hcp* and stripelike (see Figures 4b and 4c for $R_{MT} = 2/1$ and 3/1, respectively), tend to form the larger aggregation after aging. On the other hand, for the solvent system without AuTP arrangement ($R_{MT} = 1/1$ and 4/1 in Figure 4a and 4d, respectively), little enhanced aggregation was observed. Such a difference in aggregation behavior is originated from the degree of interaction of AuTP probably due to interparticle $\pi-\pi$ interaction of TPs. When the concentration of AuTP12-2.8 is larger than $\sim 5 \times 10^{-5}$ g/mL, the precipitation occurred after aging for only 1 day. It is important to note that the larger amount of precipitation appeared for the solution of $R_{MT} = 2/1$ and $R_{MT} = 3/1$. Interestingly, a significant difference in aggregation behavior was observed for the solutions of $R_{MT} = 3/1$ and 4/1 (Figure 8c and 8d, respectively), which causes stripelike arrangement and disorder, respectively (see Figure 4c and 4d, respectively), irrespective of the rather small difference in R_{MT} value.

To investigate the evidence for $\pi-\pi$ interaction of TP12 and TP8, the fluorescence (FL) spectra of AuTP12-2.8 and AuTP8-2.4 were measured in solutions with various R_{MT} values at different aging periods as shown in Figures 9 and 10, respectively. Two kinds of peaks are observed at around 384 and 438 nm, which are assigned as the emission of free TP and excimers (stacked TPs). For the fresh solution of AuTPs, the peak intensity around 438 nm was small for all the solution systems (in Figure 9), indicating that the TP units are not stacking. Significant increases in excimer peaks at 438 nm were observed depending on aging time for the solutions of $R_{MT} = 2/1$ and 3/1 (Figure 9b and c, respectively), whose solution systems caused AuTP arrangement (see Figure 4). This tendency is clearly recognized by normalized peak intensity ratio (I_{438}/I_{384}) (see insert in Figure 9). A similar tendency was observed for the AuTP8−2.4 system shown in Figure 10. Peak intensities at 384 nm are the smallest for the all fresh solutions and increased depending on the aging period. This may be due to emission quenching[49] by the interaction of TP with AuNPs in fresh solution, where TP tends to be fixed near AuTP.[31] During the aging period, the methylene units of the alkyl chains become progressively less densely packed as one moves away from the Au core, which reduces the degree of quenching for triphenylene units at 384 nm.[31] A remarkable enhancement of the fluorescent intensity around 438 nm, which is attributed to the excimer due to the π-electron overlapping mode of TP moieties,[50] was observed with an increase in the aging period for solvents with $R_{MT} = 2/1$ and 3/1 compared with those with $R_{MT} = 1/1$ and 4/1. These tendencies are clearly recognized by the change in intensity ratio of 438 to 384 nm (I_{438}/I_{384}) by the aging period (see inset in Figure 9). The results indicate that stacking of TP by $\pi-\pi$ interaction plays an important role for the self-assembly, because peaks with $\pi-\pi$ stacking at 438 nm increased extensively by aging for the solvent system where arrangement of AuTPs has been established. Similar tendencies were also observed for the AuTP8-2.4 system shown in Figure 10. These fluorescent spectral data for $\pi-\pi$ stacking of TP moieties are compatible with the tendency of aggregation by DLS (Figure 8) and MOPAC calculation for the assembly of AuTP (Figure 7). Shinkai et al. discussed the fluorescence spectra of TP derivatives.[50] According to them, two kinds of excimer emissions for TP have been reported, which originate from overlapping in eclipsed and staggered forms, where 18 and 12 carbons of TP overlap each other, respectively. The staggered overlap originates from interparticle insertion and shows an emission peak near 438 nm. We observed a peak at a similar position. On the other hand, the eclipsed overlap originates from intraparticle interaction and shows a peak near 525 nm. We cannot observe such a strong peak. Therefore, the fluorescent peak indicates that TPs on adjacent AuTPs stack to each other to lead the self-assembly, as shown in Figure 7.

Strictly speaking, the AuTPs assembly in solution and on a substrate proceeds under different conditions, because the

(48) Ipe, B. I.; Shukla, A.; Lu, H.; Zou, B.; Rehage, H.; Niemeyer, C. M. *ChemPhysChem* **2006**, *7*, 1112−1118.

(49) (a) Thomas, K. G.; Kamat, P. V. *J. Am. Chem. Soc.* **2000**, *122*, 2655−2656. (b) Kamat, P. V.; Barazzouk, S.; Hotchandani, S. *Angew. Chem., Int. Ed.* **2002**, *41*, 2764−2767.

(50) Ikeda, M.; Takeuchi, M.; Shinkai, S. *Chem. Commun.* **2003**, 1354−1355.

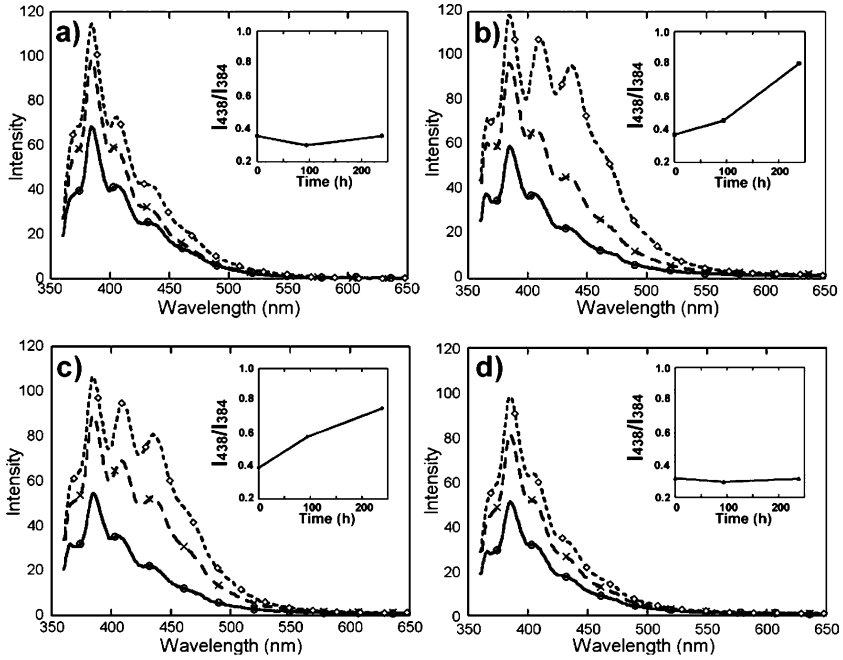

Figure 9. Time-dependent change in fluorescence spectra of AuTP12-2.8 in methanol/toluene mixed solution (1.0×10^{-5} g/mL) with R_{MT} = (a) 1/1, (b) 2/1, (c) 3/1, and (d) 4/1 at 0 h (solid line), 94 h (dashed line), and 240 h (dotted line). Inset shows the intensity ratio between the excimer (438 nm) and emission (384 nm).

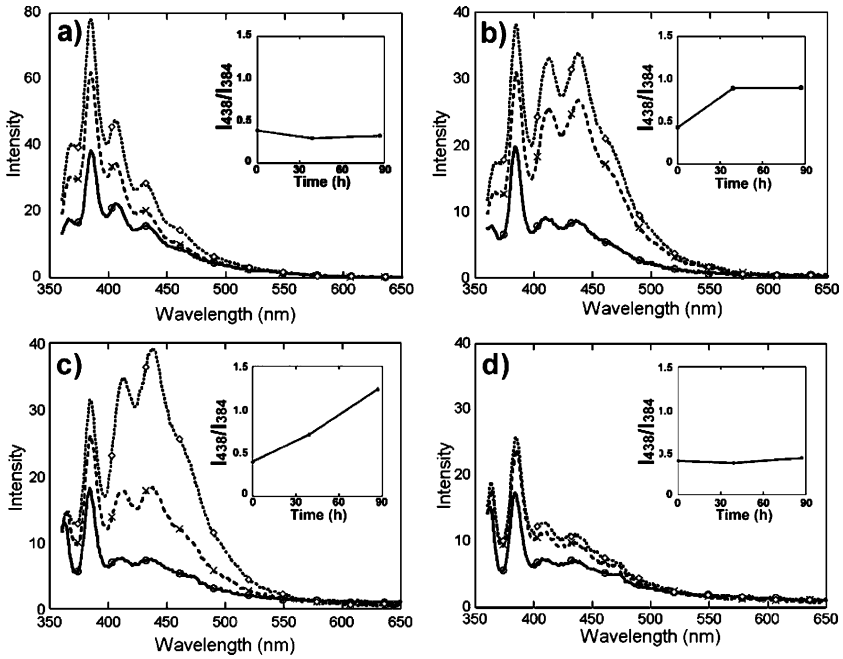

Figure 10. Time-dependent change in fluorescence spectra of AuTP8-2.4 in methanol/toluene mixed solution (1.0×10^{-5} g/mL) with R_{MT} = (a) 0/1, (b)1/1, (c)2/1, and d)3/1 at 0 h (solid line), 39 h (dashed line), and 87 h (dotted line). Inset shows the intensity ratio between the excimer (438 nm) and emission (384 nm).

arrangement is also induced by the evaporation of solvent molecules. However, we could not obtain the stripelike arrangement of AuTPs when a TEM grid was prepared by the fresh solution, whereas the 1D arrangement appeared from aged solution after more than 2 days.

3.3. Effects of Free Space among TP Ligands on Arrangements of AuTPs. It is easily understood that the space around TP moieties on the Au NPs increases with elongating the alkyl chain of the TPD*n* ligand or with reducing the core size (Figure 1). Insertions of TP ligands on adjacent AuTPs may proceed easily for the larger space between TP moieties. The space between AuTPs should be closely related to the degree of $\pi-\pi$ stacking (see Figure 7) as well as the arrangement (stripelike, *hcp*, or disorder). Heath et al. reported the volume effect of linear alkyl ligands on Au and Ag NPs in LB monolayers.[51] They deduced the arrangements of NPs depending on their outer ligand densities: the NPs with an optimum ligand density gave well-ordered *hcp* superlattices, while those with a low ligand density afforded only disorder structures.

To investigate the effect of alkyl-chain length on the self-

(51) Heath, J. R.; Knobler, C. M.; Leff, D. V. *J. Phys. Chem. B* **1997**, *101*, 189−197.

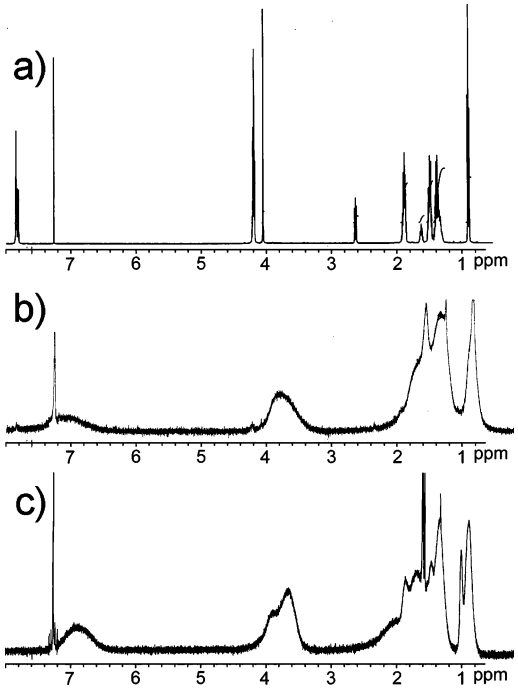

Figure 11. ^{1}H NMR spectra of (a) TPD8 (TPD12 was not shown here because of the same peaks between 8 and 3 ppm), (b) AuTP12-2.8, and (c) AuTP8-2.8 with the same core diameters in $CDCl_3$.

assembly of Au NPs, we need to compare the TEM image of AuTPs with the same gold core size (2.8 nm) but with different lengths of alkyl chain: AuTP12-2.8 (Figure 4) and AuTP8-2.8 (Figure 6). Figure 4c obviously showed a highly ordered stripelike arrangement of AuTP12-2.8, while no such arrangement was observed for AuTP8-2.8 even with different R_{MT} values (1/1−4/1, Figure 6) and even after aging for 10 days. The absence of interparticle $\pi-\pi$ stacking for AuTP8-2.8 is supported by the fluorescence spectra, which show no change in excimer peak at 438 nm for any R_{MT} solution and aging period. We have intended to investigate the effect of low ligand density (i.e., large free space) on the arrangement (*hcp* or 1D) of AuTPs by ^{1}H NMR. ^{1}H NMR spectra of AuTP8-2.8 and AuTP12-2.8 are shown in Figure 11. The ^{1}H NMR spectra of both AuTPs exhibited broadened signals due to the dipolar spin relaxation of TP ligands on the gold NP surface.[52] The broad peaks at 7.12 and 6.88 ppm which appear in Figure 11 are due to protons of aromatic rings for AuTP12-2.8 and AuTP8-2.8, respectively.

Shifts in peaks assigned to the protons in the aromatic frame (from 7.80 ppm for TPD*8* in Figure 11a to 6.88 ppm for AuTP8-2.8 in Figure 11b) and in the methoxy groups (from 4.12 to 3.68 ppm) of TP moieties reflect the highly dense packing of TP moieties in AuTP8-2.8.[53] The degree of the shift is small for AuTP12-2.8 in Figure 11b (ex: 7.8 to 7.12 ppm for protons in aromatic core) compared with that for AuTP8-2.8, suggesting that the longer alkyl chain of the TP ligand can reduce the electronic interactions among the adjacent TP moieties of AuTPs: in other words, the TP moieties can maintain their physical flexibility with larger free space (see Figure 1). Small

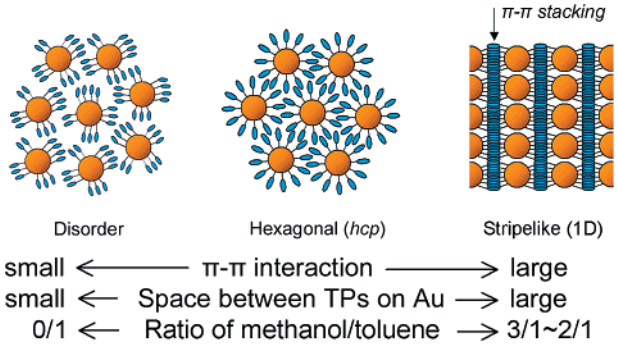

Figure 12. The possible arrangement of AuTP depends on factors investigated; $\pi-\pi$ interaction, space around TPs on Au, and solvent hydrophilicity (ratio of methanol/toluene).

broad signals at 7.80 and 4.12 ppm can also be identified to the free TPs on AuTPs. This is *not* attributable to the contamination of the free TPD12 molecules in solution because we confirm that the intensity of these signals does not change after an additional purification process by toluene/methanol to remove free TPD12 (repeated precipitation and washings for 3 additional times). Therefore, these signals at 7.80 and 4.12 ppm might originate from the free triphenylene moieties on an AuTP12 surface without $\pi-\pi$ interaction. According to the above analysis, we conclude that the alkyl chain plays a vital role in self-assembly, because it provides the large free space (low triphenylene density) for an interparticle $\pi-\pi$ interaction.

Furthermore, we investigate the effects of metal core size on space between the adjacent TP moieties on AuTPs (Figure 1c). AuTP8-2.4 compared to AuTP8-2.8 preserves sufficient space among the TP moieties, so that the TP ligands can intercalate to each other to form the *inter*molecular $\pi-\pi$ stacking, resulting in the 1D arrangement (Figure 5c). This indicates that 1D arrangement of AuTP can be realized by reducing the core size.

In order to obtain information about the $\pi-\pi$ interaction of TP in various solutions with different mixture ratios and aging periods, spectra of AuTPs were recorded in mixtures of methanol-d_4 and toluene-d_8. When using a deuterated solution with similar concentrations of AuTPs for fluorescence spectra (1.0×10^{-5} g/mL), the signal is so weak and cannot be distinguished from noise. Unfortunately, AuTPs precipitate in these deuterated solutions with higher concentration in aging solutions.

4. Conclusion

In summary, we newly synthesized a series of discotic liquid crystal molecules with a triphenylene (TP) moiety which was applied as a functional protective agent for Au NPs. The stripelike (linear 1D in row) self-assembly of AuTPs can be achieved in a 0.5 μm area due to the formation of a column structure of TP originated from strong $\pi-\pi$ stacking. Patterns of arrangements could be changed by tuning the degree of $\pi-\pi$ interaction among TPs on adjacent AuTPs to be stripelike, *hcp*, or disorder. Such $\pi-\pi$ interaction was modified by two methods. First was space between TPs on Au NPs by the preparation of AuTP with different gold core sizes and methylene lengths between the TP moiety and S atom (Figure 12). Second was solvent hydrophilicity (polarity) adjusted by the mixed ratio of methanol and toluene. In particular, for the stripelike arrangement of AuTP (see Figure 1), the following points are essential: (1) The sufficient free space around the

(52) Terrill, R. H.; Postlethwaite, T. A.; Chen, C. H.; Poon, C. D.; Terzis, A.; Chen, A.; Hutchison, J. E.; Clark, M. R.; Wignall, G.; Londono, J. D.; Superfine, R.; Falvo, M.; Johnson, C. S., Jr.; Samulski, E. T.; Murray, R. W. *J. Am. Chem. Soc.* **1995**, *117*, 12537−12548.
(53) Martin, R. B. *Chem. Rev.* **1996**, *96*, 3043−3064.

TP moieties, which easily allows the TP ligands on the adjacent Au NPs to intercalate. (2) The adjustment of the solvent hydrophilicity (mixed ratio between methanol and toluene) to promote strong *inter*molecular stacking interaction of TP moieties among AuTPs. The degree of stacking of TPs estimated by DLS, fluorescence spectra, MOPAC, and ^{1}H NMR is compatible with the arrangement of AuTPs observed by TEM. We demonstrated that the ligands with a specific property such as TP in conjunction with the circumstance of Au NPs provide a unique self-assembly structure for NPs. This strategy is applicable to a wide variety of NP systems. Concomitantly, we expect that the linear 1D row in stripes established in the present study will have potential for versatile applications in electronic and optical nanodevices, e.g., organic light-emitting diodes, field effect transistors, electroluminescences, and solar cells.[54]

Acknowledgment. This work was partially supported by a Grant-in-Aid for Scientific Research (Basic Research B, No. 17360385) from the Ministry of Culture, Education, Science and Sports, Japan and Technical Developments for PEFC Systems (No. 04003305-0) from NEDO, Japan.

JA073518C

(54) (a) Maier, S. A.; Brongersma, M. L.; Kik, P. G.; Meltzer, S.; Requicha, A. A.; Atwater, H. A. *Adv. Mater.* **2001**, *13*, 1501−1505. (b) Shiraishi, Y.; Saito, N.; Hirai, T. *J. Am. Chem. Soc.* **2005**, *127*, 12820−12822. (c) Nishikawa, T.; Torimoto, T.; Nakanishi, T.; Osaka, T.; Ohtani, B. *Chem. Phys. Lett.* **2006**, *432*, 502−507.